Hyperglycemia-Induced Protein Kinase C β_2 Activation Induces Diastolic Cardiac Dysfunction in Diabetic Rats by Impairing Caveolin-3 Expression and Akt/eNOS Signaling

Shaoqing Lei,[1] Haobo Li,[1] Jinjin Xu,[1] Yanan Liu,[1] Xia Gao,[1] Junwen Wang,[2,3] Kwok F.J. Ng,[1,3] Wayne Bond Lau,[4] Xin-liang Ma,[4] Brian Rodrigues,[5] Michael G. Irwin,[1,3] and Zhengyuan Xia[1,3]

Protein kinase C (PKC)β_2 is preferably overexpressed in the diabetic myocardium, which induces cardiomyocyte hypertrophy and contributes to diabetic cardiomyopathy, but the underlying mechanisms are incompletely understood. Caveolae are critical in signal transduction of PKC isoforms in cardiomyocytes. Caveolin (Cav)-3, the cardiomyocyte-specific caveolar structural protein isoform, is decreased in the diabetic heart. The current study determined whether PKCβ_2 activation affects caveolae and Cav-3 expression. Immunoprecipitation and immunofluorescence analysis revealed that high glucose (HG) increased the association and colocalization of PKCβ_2 and Cav-3 in isolated cardiomyocytes. Disruption of caveolae by methyl-β-cyclodextrin or Cav-3 small interfering (si)RNA transfection prevented HG-induced PKCβ_2 phosphorylation. Inhibition of PKCβ_2 activation by compound CGP53353 or knockdown of PKCβ_2 expression via siRNA attenuated the reductions of Cav-3 expression and Akt/endothelial nitric oxide synthase (eNOS) phosphorylation in cardiomyocytes exposed to HG. LY333531 treatment (for a duration of 4 weeks) prevented excessive PKCβ_2 activation and attenuated cardiac diastolic dysfunction in rats with streptozotocin-induced diabetes. LY333531 suppressed the decreased expression of myocardial NO, Cav-3, phosphorylated (p)-Akt, and p-eNOS and also mitigated the augmentation of O_2^-, nitrotyrosine, Cav-1, and iNOS expression. In conclusion, hyperglycemia-induced PKCβ_2 activation requires caveolae and is associated with reduced Cav-3 expression in the diabetic heart. Prevention of excessive PKCβ_2 activation attenuated cardiac diastolic dysfunction by restoring Cav-3 expression and subsequently rescuing Akt/eNOS/NO signaling. ***Diabetes*** **62:2318–2328, 2013**

Cardiovascular disease is the leading cause of diabetes-related death (1). While most diabetic heart failure etiology concerns coronary disease associated with atherosclerosis, a diabetes-associated cardiomyopathy has been reported in humans (2) and animal models of type 1 (3) and type 2 (4) diabetes. Numerous studies by our group (5,6) and others (7,8) suggest the involvement of excess expression or activation of protein kinase C (PKC)β_2 in the development and progression of diabetic cardiomyopathy. Moreover, inhibition of PKCβ activation improves cardiac function in diabetic animals (9,10). Despite these observations, the underlying mechanism by which PKCβ_2 activation exerts deleterious effects in the diabetic myocardium remains unclear.

PKCβ_1 and PKCβ_2 are two of the classical isoforms (α, β, and γ) of PKC (11). Of the two isoforms, PKCβ_2 is preferentially overexpressed in the myocardium of patients (12) or animals (10) with diabetes. PKCβ_2 activation has been implicated in diabetes-associated abnormalities via inhibition of Akt-dependent endothelial nitric oxide (NO) synthase (eNOS) activity (13), and restoration of Akt-eNOS-NO signaling has been shown to attenuate diabetic cardiomyopathy and myocardial dysfunction (14). Altered caveolae formation may potentially be the root cause of such inhibition. Caveolae, lipid rafts formed by small plasma membrane invaginations, serve as platforms modulating signal transduction pathways (e.g., PKC isoforms [15]) via molecules docked with caveolin (Cav), a major constituent protein associated with caveolae. Of the three Cav isoforms identified in mammalian caveolae, Cav-3 is mainly expressed in cardiac muscle and is essential for proper formation of cardiomyocyte caveolae (16). Interestingly, in cardiomyocytes, eNOS localizes to Cav-3 (17), permitting eNOS activation by cell surface receptors and cellular surface NO release for intercellular signaling (17). Therefore, NO is an endogenous inhibitor of hypertrophic signaling (18), and Cav-3 is important for maintaining NO function. Additionally, Cav-3 has been demonstrated to inhibit growth signaling in the hearts of nondiabetic subjects (19). Thus, any alteration in Cav-3 expression in the diabetic condition may participate in the pathogenesis of diabetic cardiomyopathy, which is supported by findings that decreased cardiac Cav-3 expression is detected in rats with chronic streptozotocin (STZ)-induced diabetes (20,21). In the current study, we hypothesize that PKCβ_2 activation induced by hyperglycemia promotes caveolae dysfunction with associated signaling abnormality. Our data suggest that excessive PKCβ_2 activation during diabetes reduces Cav-3 expression, with subsequent decreased Akt/eNOS signaling, which ultimately and negatively affect cardiac remodeling and function.

RESEARCH DESIGN AND METHODS

Induction of diabetes and drug treatment. Male Sprague-Dawley rats (aged 8 weeks) weighing 260 ± 10 g equilibrated to surroundings for 3 days before experiments. Diabetes was induced via single tail vein injection of STZ (60 mg/kg; Sigma, St. Louis, MO) dissolved in citrate buffer (0.1 mol/L, pH 4.5), while control rats were injected with an equal volume of citrate buffer alone. One

From the [1]Department of Anesthesiology, University of Hong Kong, Hong Kong, China; the [2]Department of Biochemistry, University of Hong Kong, Hong Kong, China; the [3]Shenzhen Institute of Research & Innovation, University of Hong Kong, Shenzhen, China; the [4]Department of Emergency Medicine, Thomas Jefferson University, Philadelphia, Pennsylvania; and the [5]Faculty of Pharmaceutical Sciences, University of British Columbia, Vancouver, British Columbia, Canada.
Corresponding author: Zhengyuan Xia, zyxia@hku.hk.
Received 8 October 2012 and accepted 28 February 2013.
DOI: 10.2337/db12-1391
M.G.I. and Z.X. share senior authorship.

week after STZ injection, rats exhibiting hyperglycemia (blood glucose ≥16.7 mmol/L) were considered diabetic and were subjected to outlined experiments. One week after diabetes induction, rats were treated with vehicle or PKCβ inhibitor LY333531 (also named ruboxistaurin, a drug that has been approved by the U.S. Food and Drug Administration for the prevention of vision loss in patients with diabetic retinopathy [22]) by oral gavage for 4 weeks at a dose of 1 mg/kg/day (demonstrated to adequately inhibit PKCβ activation in rat heart and vasculature [23,24]). This model was chosen based on our most recent study (25) and a study of others (26) showing that STZ diabetic rats developed cardiac dysfunction 35 days after STZ injection, with concomitant cardiomyocyte hypertrophy and cardiac fibrosis formation (25)—two major features of diabetic cardiomyopathy. After 4 weeks' treatment, cardiac functions were determined; the rats were then deeply anesthetized with sodium pentobarbital (65 mg/kg), and hearts were either rapidly excised for cardiomyocyte isolation or frozen in liquid nitrogen for later analysis. Subgroups of control and untreated diabetic rats were terminated at 8 weeks of STZ-induced diabetes, and heart tissue samples were processed to analyze changes of cardiac PKCβ_2 and Cav-3 at a relatively later phase of the disease. All experiments performed conformed to the Guide for the Care and Use of Laboratory Animals, published by the National Institutes of Health (NIH publication no. 86–23, revised 1996), and were approved by the Institutional Animal Care and Use Committee of Hong Kong University.

Echocardiography. At the conclusion of 4 weeks' treatments, transthoracic echocardiography was performed at experiment termination via a 17.5-MHz linear array transducer system (Vevo 770, High Resolution Imaging System; VisualSonics, Toronto, Ontario, Canada), and left ventricular (LV) dimensions and LV diastolic and systolic function were assessed by M-mode and Doppler echocardiography as we previously described (25). LV internal dimensions at end systole (LVIDs) and diastole (LVIDd) were used to calculate fractional shorting (FS) by the following formula: FS (%) = (LVIDd − LVIDs)/LVIDd × 100%. LV posterior wall dimensions at end diastole (LVPWd) and systole (LVPWs) were used to calculate fractional LV posterior wall thickening (FLVPW) by the following formula: LVPW(%) = LVPWs − LVPWd/LVPWd × 100%. The peak velocity of early (E) and late (A) diastolic filling was used to calculate the ratio of E and A (E/A). LV end diastolic volume (LVVd) and end systolic volume (LVVs) were used to calculate ejection fraction (EF) by the following formula: EF (%) = LVVd − LVVs/LVVd × 100%. The heart rate (HR), systolic interventricular septal thickness, diastolic interventricular septal thickness, LV isovolumic relaxation time (IVRT), and stroke volume (SV) were also monitored. All echocardiographically derived measures were obtained by averaging the readings of three consecutive beats.

Measurement of cardiomyocytes cross-sectional area. After the completion of 4 weeks' treatment, cardiomyocyte cross-sectional diameters were assessed by hematoxylin-eosin–stained paraffin-embedded sections of left ventricles (1–2 μm) longitudinally orientated to the muscle fibers in the subendocardium and subepicardium as previously described (6). Cross-sectional areas were randomly selected in five fields that visualized capillary profiles and nuclei. Images of the left ventricle sections were captured by an Axioplus image-capturing system (Zeiss) and analyzed by Axiovision Rel. 4.5 image-analyzing software. A minimum of 150 cells per animal was chosen for analysis.

Preparation of isolated rat ventricular cardiomyocytes. Calcium-tolerant cardiomyocytes were prepared from rat ventricles via a modified method as

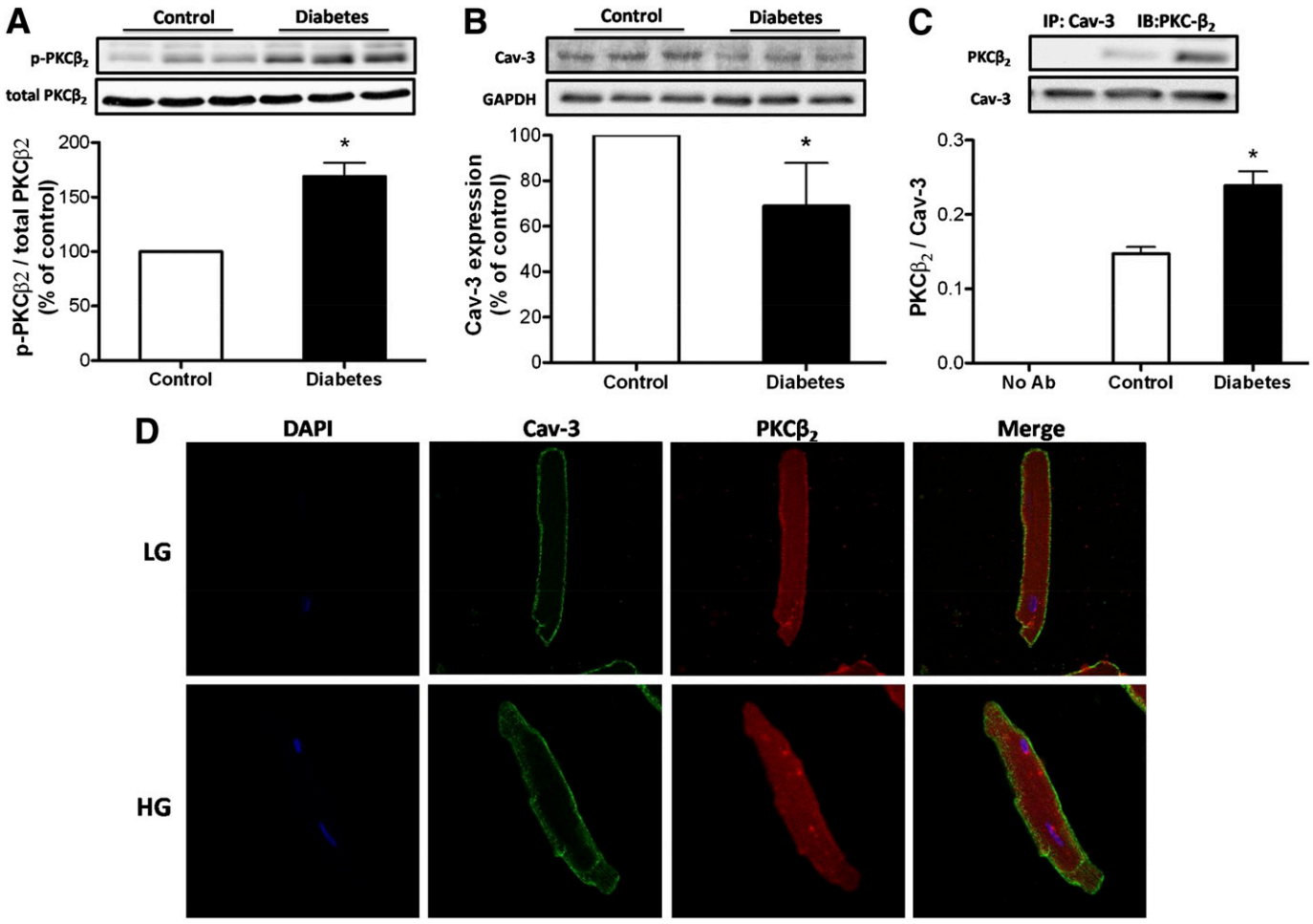

FIG. 1. Expression of PKCβ_2 and Cav-3 in cardiomyocytes isolated from control and STZ-induced diabetic rats (8 weeks). *A*: Representative Western blot demonstrating p-PKCβ_2 (Ser^{660}) and total PKCβ_2 expression. *B*: Representative Western blot demonstrating Cav-3 expression with glyceraldehyde-3-phosphate dehydrogenase (GAPDH) as loading control. *C*: Cell lysates containing equal amounts of total protein were subjected to immunoprecipitation (IP) with anti–Cav-3 antibody (Ab) and analyzed by immunoblot (IB) with PKCβ_2 and Cav-3 antibody. All results are expressed as means ± SEM. n = 6–8 per group. *$P < 0.05$ vs. control. *D*: Confocal laser microscopic image of adult rat cardiomyocytes in response to HG. Isolated cardiomyocytes from nondiabetic rats were incubated with LG or HG for 36 h and underwent standard immunofluorescent staining with PKCβ_2 and Cav-3 antibodies (see RESEARCH DESIGN AND METHODS).

previously described (27). Cells isolated from a single rat heart were plated on Matrigel-coated culture dishes and allowed to recover for 3 h. Cultured ventricular cardiomyocytes were incubated in low glucose (LG) (5.5 mmol/L), high glucose (HG) (25 mmol/L), or mannitol/glucose (19.5 mmol/L mannitol plus 5.5 mmol/L glucose) at 37°C in Medium 199 (Gibco, Grand Island, NY) containing various treatments and then snap-frozen in liquid nitrogen for future analysis. Lactate dehydrogenase (LDH) release (a measure of cell injury) in culture medium was detected via a commercial LDH kit (Roche, Mannheim, Germany).

Immunoprecipitation. Isolated cardiomyocytes were homogenized in lysis buffer. A total of 500 μg cell extracts were subjected to immunoprecipitation with 2 μg Cav-3 primary antibody in the presence of 20 μL protein A/G plus-agarose. After extensive PBS washes, the immunoprecipitates were denatured with 1× sodium dodecyl sulfate loading buffer and subjected to analysis for PKCβ$_2$ expression by Western blot as described below.

Immunofluorescence. Isolated cardiomyocytes were plated on Matrigel precoated glass coverslips, incubated either in LG or HG in Medium 199 for 36 h, and fixed in ice-cold acetone for 5 min. The fixed cells were blocked in PBS with Tween 20 (PBST) with 10% goat serum and 1% BSA for 30 min and further incubated with a mixture of mouse against rat Cav-3 antibody (1:50; Santa Cruz Biotechnology, Santa Cruz, CA) and rabbit against rat PKCβ$_2$ antibody (1:100; Santa Cruz Biotechnology) in 1% BSA in PBST in a humidified chamber for 1 h at room temperature. After three PBST washings, the cells were incubated for 1 h with a mixture of Alexa Fluor 488 goat anti-mouse IgG and Alexa Fluor 594 goat anti-rabbit IgG (1:2,000; Invitrogen, Carlsbad, CA). Cells were washed three times and prepared for confocal laser scanning microscopic imaging with mounting medium with DAPI (Vector Laboratories, Burlingame, CA).

PKCβ$_2$ siRNA and Cav-3 siRNA studies in H9C2 cells. Embryonic rat cardiac H9C2 cells were maintained in Dulbecco's modified Eagle's medium containing 10% FBS in a humidified atmosphere (5% CO_2) at 37°C. Commercial PKCβ$_2$ siRNA and Cav-3 siRNA (Santa Cruz Biotechnology) were used for inhibition of both PKCβ$_2$ and Cav-3 expression per the manufacturer's protocol. After transfection with control, PKCβ$_2$, or Cav-3 siRNA, cells were incubated in either LG or HG in Dulbecco's modified Eagle's medium for 36 h and snap-frozen in liquid nitrogen.

Determination of myocardial levels of NO, O_2^-, and nitrotyrosine. Frozen heart tissues were pulverized separately with mortar and pestle in liquid nitrogen, homogenized in ice-cold PBS, and centrifuged at 3,000*g* for 15 min at 4°C for supernatant collection. The supernatant protein concentration was determined via a Lowry assay kit (Bio-Rad, Hercules, CA). Concentrations of nitrites (NO_2^-) and nitrates (NO_3^-), the stable end products of NO, were determined by the Griess reaction as previously described (28). NO levels were expressed as nanomoles per microgram of protein. Myocardial O_2^- production was determined via lucigenin chemiluminescence method (29,30). The supernatant samples were loaded with dark-adapted lucigenin (5 μmol/L) and read in 96-well microplates by luminometer (GloMax; Promega) with and without pretreatment with the NOS inhibitor L-N^G-nitroarginine methyl ester (L-NAME) (100 μmol/L [15]) for 30 min at room temperature. Light emission, expressed as mean light units/min/100 μg protein, was recorded for 5 min. Myocardial nitrotyrosine levels (micrograms per milligram protein) in the collected supernatant were determined by chemiluminescence detection via the Nitrotyrosine Assay kit per the manufacturer's protocol (Millipore).

Separation of cytosol and membrane fractions of heart tissues. For characterization of subcellular distributions of targeted proteins, cytosol and membrane fractions of cardiac tissue lysate were separated by ultracentrifugation as previously described (5). Cytosol and membrane fractions were denatured by 5× sodium dodecyl sulfate loading buffer and subjected to analysis for PKCβ$_1$ and PKCβ$_2$ expression by Western blot as described below.

Isolation of Cav-rich fractions. Caveolae were isolated by discontinuous sucrose gradient centrifugation as previously described (21). Each heart sample gradient was separated into 12 fractions. Fractions 4–6 were considered the lipid raft fractions, and fractions 8–12 were considered the heavier fractions. Equal protein amounts were loaded for Western blot analysis.

Western blot analysis. Equal protein amounts from isolated cardiomyocytes, H9C2 cells, and rat heart homogenate were resolved by 7.5–12.5% SDS-PAGE

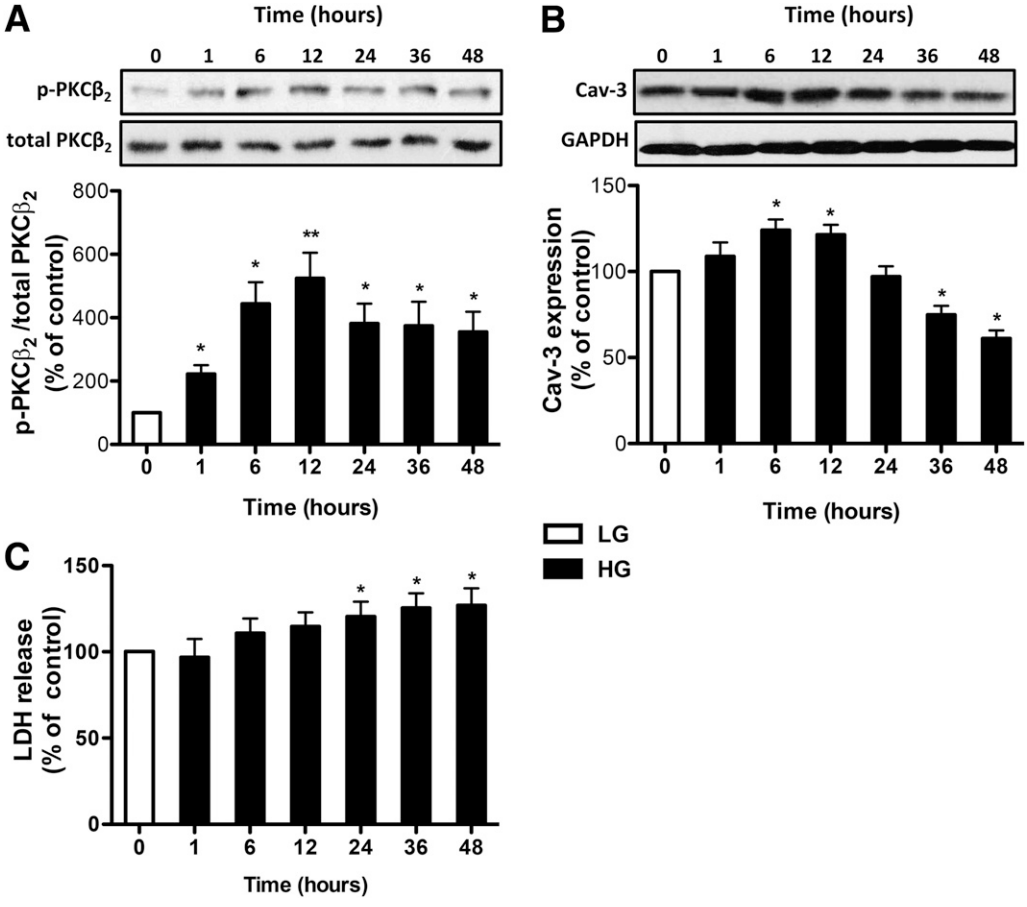

FIG. 2. Effects of HG upon p-PKCβ$_2$ (Ser^{660}) and Cav-3 expression and LDH release in cultured cardiomyocytes over time. Representative Western blot of p-PKCβ$_2$ (Ser^{660}) expression in comparison with total-PKCβ$_2$ (*A*) and Cav-3 (*B*) expression with glyceraldehyde-3-phosphate dehydrogenase (GAPDH) as loading control. *C*: Effects of HG upon LDH release. **P* < 0.05, ***P* < 0.01 vs. control (time "0") group.

and subsequently transferred to polyvinylidene fluoride membrane for immunoblot analysis as previously described (31).

Statistical analysis. Densitometry was obtained by image analysis software (Bio-Rad). All values are presented as means ± SEM. Comparisons between multiple groups were made by one-way ANOVA followed by Tukey test for multiple comparisons. Statistical analysis was performed by GraphPad Prism (GraphPad Software, San Diego, CA). P values <0.05 were considered significant.

RESULTS

Expression and association of PKCβ$_2$ and Cav-3 in cardiomyocytes isolated from diabetic rats. We previously reported activation of the PKCβ$_2$, but not PKCβ$_1$, isoform in the diabetic heart (6). In the current study, we examined whether PKCβ$_2$ activation was associated with abnormal Cav-3 expression, a muscle-specific marker of caveolae (16). Diabetes moderately increased PKCβ$_2$ phosphorylation on Thr^{642} residue (data not shown), but the increase in phosphorylation of PKCβ$_2$ was most profound at Ser^{660}, without influencing total PKCβ$_2$, resulting in a markedly increased ratio of phosphorylated PKCβ$_2$ to total PKCβ$_2$ (Fig. 1*A*). Decreased Cav-3 expression was observed in cardiomyocytes isolated from 8-week diabetic rat hearts compared with age-matched controls (Fig. 1*B*). We next examined the relationship between Cav-3 and PKCβ$_2$ by immunoprecipitation experiments in isolated cardiomyocytes. While a small amount of PKCβ$_2$ remained constitutively associated with Cav-3 during basal conditions, the diabetic condition increased its association with Cav-3 (Fig. 1*C*). To confirm our findings, we used confocal immunofluorescence staining. Limited PKCβ$_2$ was present during basal conditions in association with Cav-3 in the cell membrane (indicated by scant yellow punctate staining of the cell periphery); 36 h of HG stimulation significantly increased regions of colocalization between PKCβ$_2$ and Cav-3 compared with LG stimulation (Fig. 1*D*).

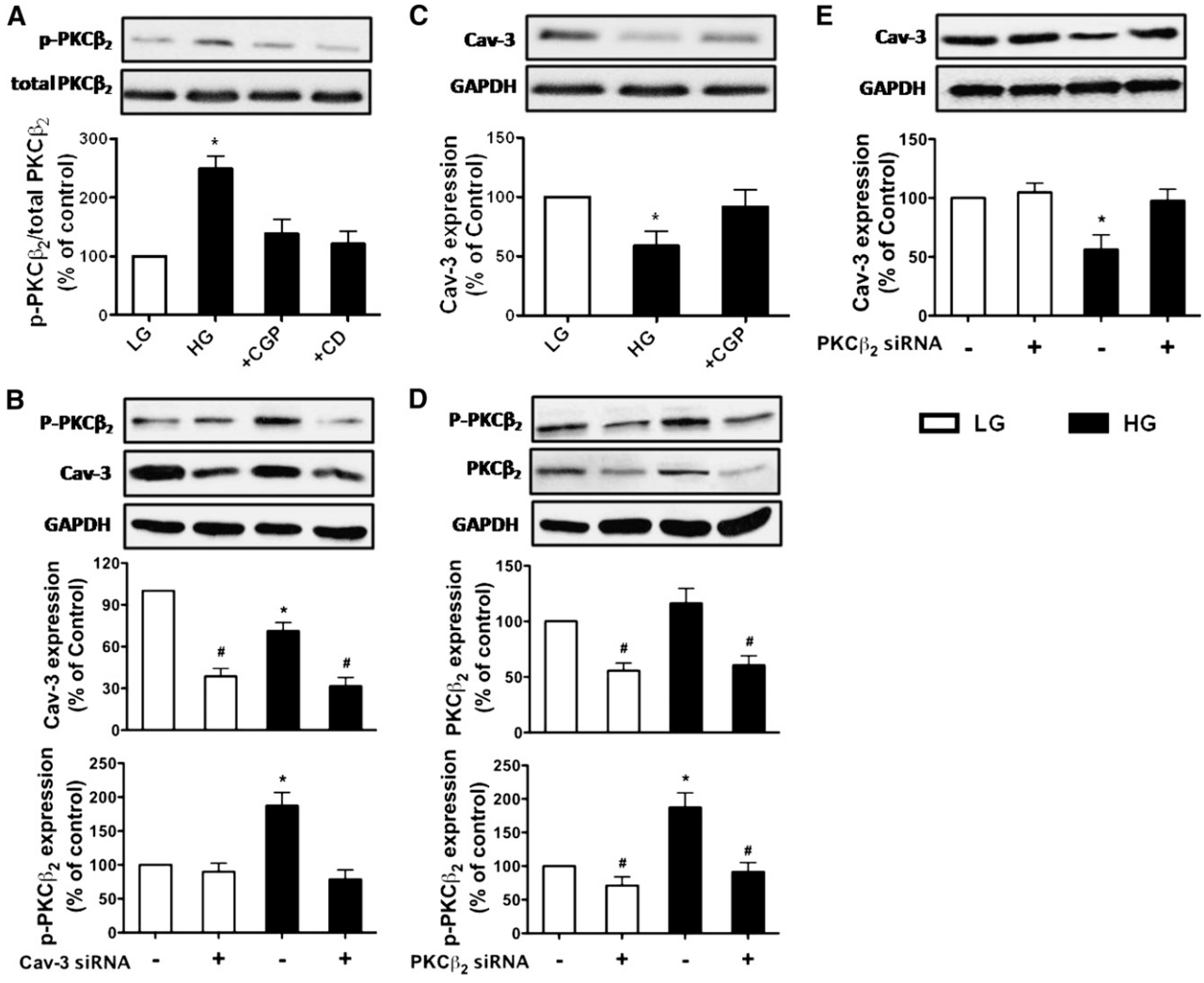

FIG. 3. Expression of p-PKCβ$_2$ and Cav-3 in cultured cardiomyocytes and H9C2 cells after various treatments in LG (5.5 mmol/L) or HG (25 mmol/L) conditions for 36 h. *A*: Representative Western blot demonstrating p-PKCβ$_2$ (Ser^{660}) in comparison with total PKCβ$_2$ in cardiomyocytes exposed to HG in the presence of a selective PKCβ$_2$ inhibitor, CGP (1 μmol/L), or CD (10 μmol/L). *B*: Representative Western blot demonstrating p-PKCβ$_2$ and Cav-3 expression in H9C2 cells transfected with Cav-3 siRNA exposed to LG or HG. *C*: Representative Western blot demonstrating Cav-3 expression in cultured cardiomyocytes exposed to HG in the presence of CGP (1 μmol/L). *D*: Representative Western blot demonstrating p-PKCβ$_2$, total PKCβ$_2$ expression, and Cav-3 expression in H9C2 cells transfected with PKCβ$_2$ siRNA in LG or HG conditions. Glyceraldehyde-3-phosphate dehydrogenase (GAPDH) served as loading control. All results are expressed as means ± SEM. $n = 7$. *$P < 0.05$ vs. all other groups, #$P < 0.05$ vs. control and siRNA-treated groups.

Effect of HG on expression and association of p-PKCβ2 and Cav-3 in isolated cardiomyocytes over time. HG conditions significantly increased the ratio of p-PKCβ2 to total PKCβ2 (indicating PKCβ2 activation) in cardiomyocytes within 1 h for up to 48 h (Fig. 2*A*). Peak increase in the ratio of p-PKCβ2 to total PKCβ2 occurred after 12 h HG exposure. The osmotic control mannitol exerted no effects upon p-PKCβ2 to total PKCβ2 and Cav-3 expression (data not shown). In contrast to the quick increase of phosphorylated (p)-PKCβ2/total PKCβ2 as early as 1 h after HG exposure, Cav-3 expression did not significantly increase until 6–12 h after HG exposure, reduced to basal levels within 24 h, and significantly decreased 36–48 h after initial HG exposure (Fig. 2*B*). Cardiomyocyte LDH release significantly increased 24 h after HG exposure, with a rising tendency continuing 36–48 h after initial HG exposure (Fig. 2*C*).

Hyperglycemia-induced PKCβ2 activation involves caveolae and is associated with reduced Cav-3 expression. We next investigate the interplay between PKCβ2 activation and caveolae (and Cav-3) under hyperglycemic conditions. Given that PKCβ1 activation induced by HG requires caveolae in primary mesangial cells (32), we determined whether caveolae are crucial in HG-induced PKCβ2 activation in isolated cardiomyocytes from nondiabetic rats. As shown in Fig. 3*A*, phosphorylation of PKCβ2 induced by HG was prevented by either the selective PKCβ2 inhibitor CGP-53353 (1 μmol/L; Sigma-Aldrich

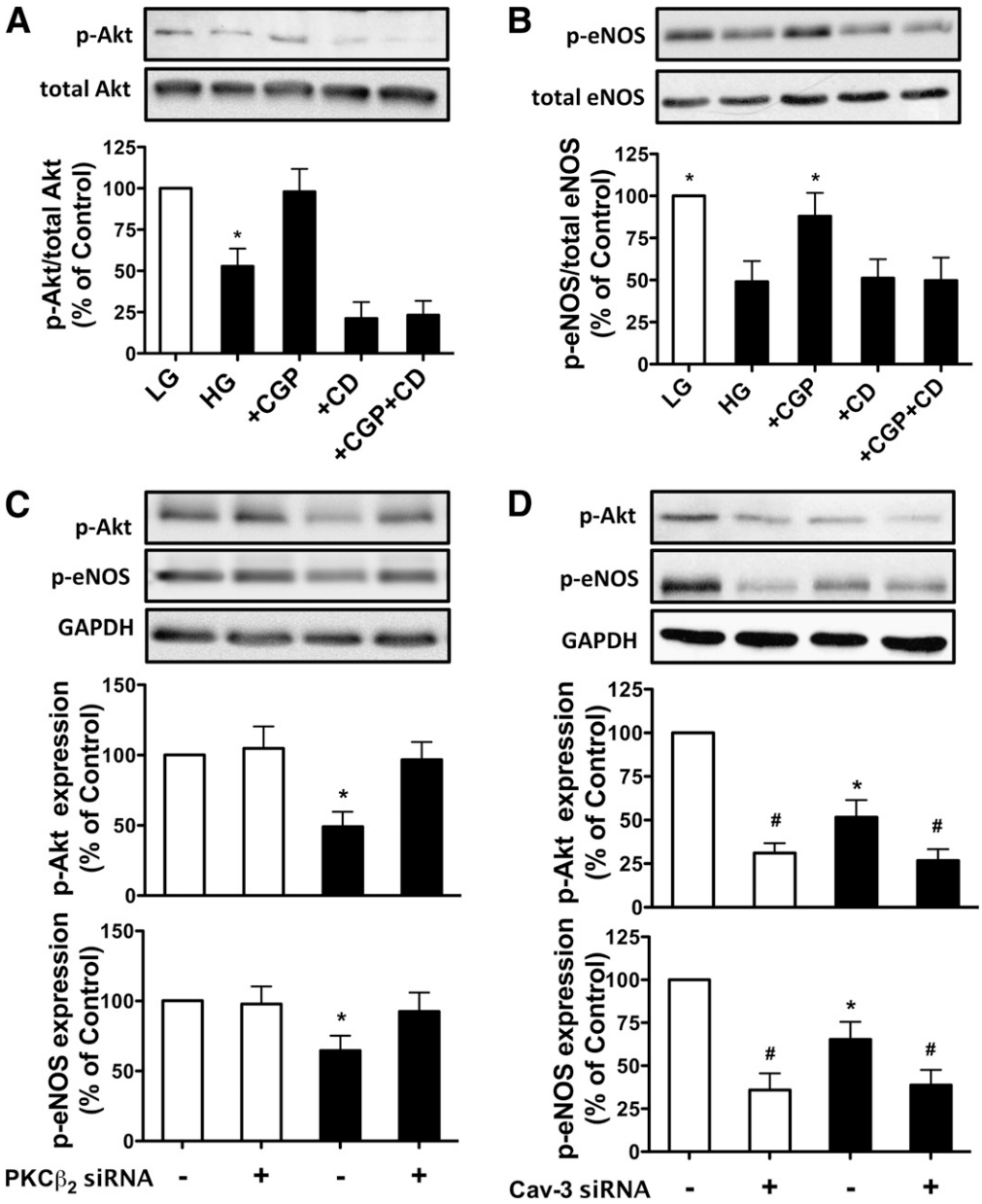

FIG. 4. Expression of p-Akt (Ser 473) and p-eNOS (Ser 1177) in cultured cardiomyocytes and H9C2 cells in various treatments in LG (□) (5.5 mmol/L) or HG (■) (25 mmol/L) conditions for 36 h. Representative Western blot demonstrating p-Akt in comparison with total Akt (*A*) and p-eNOS in comparison with total eNOS in cardiomyocytes exposed to HG in the presence of selective PKCβ2 CGP (1 μmol/L), CD (10 μmol/L), or CGP+CD combination (*B*). Representative Western blot demonstrating p-Akt and p-eNOS expression in H9C2 cells transfected with PKCβ2 siRNA (*C*) or Cav-3 siRNA (*D*) in LG or HG conditions. Glyceraldehyde-3-phosphate dehydrogenase (GAPDH) served as loading control. All results are expressed as means ± SEM. $n = 7$. *$P < 0.05$ vs. all other groups, #$P < 0.05$ vs. control and siRNA-treated groups.

[IC_{50} values are 0.41 and 3.8 μmol/L, respectively, for PKCβ$_2$ and PKCβ$_1$]) or methyl-β-cyclodextrin (CD) (50 μmol/L), a disrupter of cholesterol-rich caveolae (33). To determine whether Cav-3 is required for PKCβ$_2$ activation, we subjected H9C2 cells treated with rat-specific Cav3 small interfering (si)RNA to both LG and HG conditions. siRNA-mediated reduction of Cav-3 expression by ~60% (Fig. 3*B*) prevented augmented phosphorylation of PKCβ$_2$ in HG conditions. No effects upon PKCβ$_2$ phosphorylation were observed in cells exposed to LG (Fig. 3*B*). We also determined whether excessive PKCβ$_2$ activation induced by HG is associated with reduced Cav-3 expression. Selective inhibition of PKCβ$_2$ activation by CGP reversed the reduction of Cav-3 expression in primary cardiomyocytes exposed to HG (Fig. 3*C*). Similarly, in H9C2 cells, knockdown of PKCβ$_2$ by siRNA reduced PKCβ$_2$ phosphorylation in cells incubated in LG and HG conditions (Fig. 3*D*) and attenuated decreased Cav-3 expression in cells exposed to HG, with no impact upon Cav-3 expression in cells exposed to LG (Fig. 3*E*).

Hyperglycemia-induced activation of PKCβ$_2$ is associated with caveolae-modulated Akt/eNOS signaling. Next, we investigated the impact of PKCβ$_2$ activation by HG in the downstream signaling molecules Akt and eNOS, both of which are modulated by Cavs (34). Cardiomyocytes incubated in HG exhibited decreased phosphorylation of Akt at Ser^{473} and eNOS at Ser^{1177}, and these decreases were reversed by CGP treatment (Fig. 4*A* and *B*). Caveolar disruption by CD further exaggerated HG-mediated reduction of Akt phosphorylation (Fig. 4*A*) but did not further exacerbate HG-induced reduction of p-eNOS expression (Fig. 4*B*). However, CGP-mediated restoration of eNOS phosphorylation in HG-treated cardiomyocytes was abolished during concomitant CD treatment (Fig. 4*B*). For confirmation of the relative effects of PKCβ$_2$ and Cav-3 upon HG-mediated changes in p-AKT and p-eNOS, H9C2 cells were subject to both PKCβ$_2$ and Cav-3 knockdown by siRNA. PKCβ$_2$ knockdown significantly increased the phosphorylation of Akt and eNOS in HG-treated cells—effects that were not observed in LG-treated cells (Fig. 4*C*). Knockdown of Cav-3 resulted in further reduced expression of both p-Akt and p-eNOS in both LG- and HG-treated cells (Fig. 4*D*).

Inhibition of PKCβ$_2$ activation by LY333531 attenuates cardiac caveolar dysfunction in diabetic rats. To further investigate the role of PKCβ$_2$ activation in diabetes-induced abnormalities, we treated STZ-induced diabetic rats with the PKCβ inhibitor LY333531 for 4 weeks. PKCβ$_2$, but not PKCβ$_1$, isoform was excessively activated in the diabetic heart, as demonstrated by increased membrane translocation of PKCβ$_2$ but not PKCβ$_1$—a phenomenon inhibited by LY333531 (Fig. 5*A*). PKCβ2 inhibitor LY333531 administration suppressed augmented whole-heart Cav-1 expression (Fig. 5*B*) and prevented whole-heart decreased Cav-3 expression (Fig. 5*C*). Caveolae fractions were isolated via

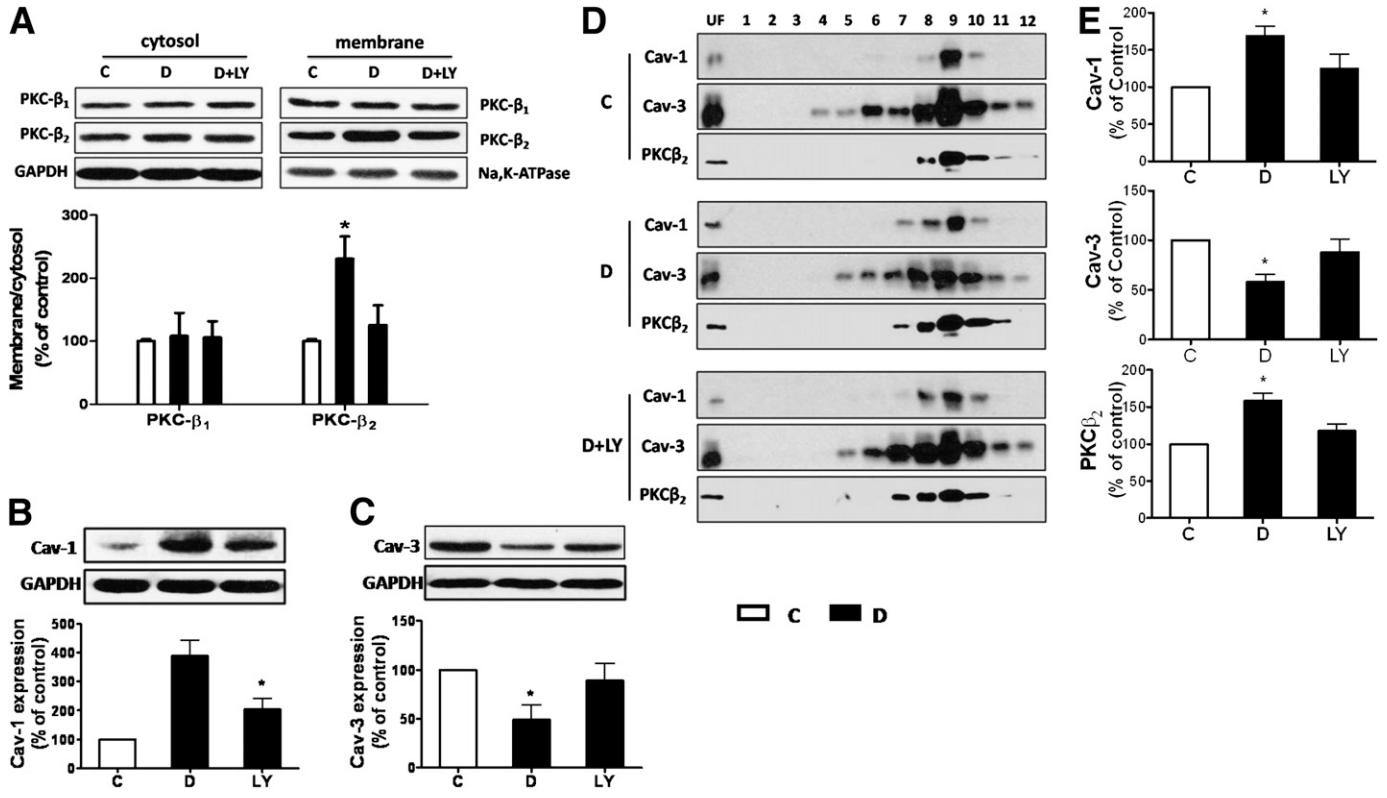

FIG. 5. Effects of PKCβ inhibitor (LY333531) treatment upon subcellular distributions of PKCβ$_1$ and PKCβ$_2$ and expression levels of Cav-1 and Cav-3 in total heart preparations and various isolated cellular fractions. Control (C) or rats with STZ-induced diabetes were treated with PKCβ inhibitor LY333531 (1 mg/kg/day, D+LY) or control (D) by oral gavage for 4 weeks. *A*: Representative Western blot demonstrating PKCβ$_1$ and PKCβ$_2$ protein expression. Glyceraldehyde-3-phosphate dehydrogenase (GAPDH) and Na-K-ATPase served as loading controls in cytosol fractions or membrane fractions, respectively. *Bottom panel*: Membrane-to-cytosol ratio as indexes of PKCβ isoform translocation. Representative Western blot demonstrating Cav-1 (*B*) and Cav-3 (*C*) content in total heart preparations. *D*: Sucrose gradient centrifugation isolated caveolae-enriched fractions. Aliquots containing equal amounts of protein or a volume equal to that of the fraction with the least detectable amount of protein for "protein-free" fractions (1,2) and unfractionated samples were probed for Cav-1, Cav-3, and PKCβ$_2$ immunoreactivity. *E*: Cav-1 and Cav-3 and PKCβ$_2$ expression in all the fractions (1–12) were calculated by relative densitometric values and expressed as percentage of control. All results are expressed as means ± SEM. $n = 7$. *$P < 0.05$ vs. all other groups.

discontinuous sucrose gradient centrifugation of whole cell lysates. Cav-1 was found predominantly in fractions 8–10, whereas Cav-3 was located within both lipid fractions (4–6) and heavier fractions (8–12). PKCβ$_2$ was predominantly coexpressed within Cav-3–rich fractions (Fig. 5*D*). Densitometric analysis of all fractions (1–12) demonstrated that PKCβ2-inhibitor LY333531 significantly reduced augmented Cav-1 and PKCβ$_2$ expression and suppressed decreased Cav-3 expression in diabetes (Fig. 5*E*).

Inhibition of PKCβ$_2$ activation by LY333531 attenuates diastolic dysfunction in diabetic rats. At the end of the treatment period, untreated diabetic rats had significantly elevated blood glucose and reduced body weight and heart weight compared with control rats, which were not altered by LY333531 treatment (Table 1). However, the ratio of heart weight to body weight, an indirect index of myocardial hypertrophy, in the untreated diabetic rats was significantly higher than that in the control rats, which was significantly attenuated by LY333531 treatment (Table 1). Further, the LV cardiomyocyte cross-sectional areas as assessed in hematoxylin-eosin–stained cardiac sections in the untreated diabetic rats (478.8 ± 58.9 μm^2) were significantly bigger than in the control rats (256.7 ± 37.9 μm^2) and significantly attenuated by LY333531 treatment (329.5 ± 47.7 μm^2), showing that LY333531 can attenuate cardiomyocyte hypertrophy in diabetes. We further determined rat cardiac function via echocardiography. As shown in Table 1, no significant change in FS, FLVPW, or EF was observed among all experimental groups (although nonsignificant decreased values were recorded in the untreated diabetic group). Such data suggest preserved systolic function at 5 weeks in diabetic rats used in our model. However, diastolic dysfunction was manifested. The HR and the E/A ratio were significantly decreased in diabetic rats as a consequence of significant reduction of E velocity and enhancement of A velocity that was concomitant with significant increase in LV IVRT and reductions in LVVd and SV. Four weeks' treatment with LY333531 restored the values of E/A, IVRT, LVVd, and SV to levels that were comparable with those in the control rats but without significant effect upon HR.

LY333531 ameliorated diabetes-induced derangements of myocardial NO, O_2^-, and nitrotyrosine content and reverted changes in cardiac Akt, eNOS, and inducible NOS. Diabetes is associated with decreased NO levels and increased O_2^- and nitrotyrosine production (14,35), agents of oxidative and nitrative stress. For determination of whether LY333531 conferred cardioprotection in part by reducing oxidative and nitrative stress in diabetes, the levels of NO, O_2^-, and nitrotyrosine in diabetic heart tissues were assessed. The diabetic condition significantly decreased NO levels (Fig. 6*A*) and increased O_2^- (Fig. 6*B*) and nitrotyrosine production (Fig. 6*C*) in cardiac tissues. LY333531 suppressed all of these derangements. Further studies revealed that the diabetes-induced augmented O_2^- levels could be blocked by the NOS inhibitor L-NAME (100 μmol/L) (Fig. 6*B*), suggesting an NOS-dependent mechanism for O_2^- accumulation. We next investigated related signaling molecules, including Akt, eNOS, and inducible NOS (iNOS). The diabetic condition did not affect total cardiac Akt and eNOS expression but significantly decreased p-Akt (Ser^{473}) and p-eNOS (Ser^{1177}) expression, both of which were reversed by LY333531 (Fig. 6*D* and *E*). Consistent with a recent study (36), our results demonstrate that diabetes increased myocardial iNOS (an adverse marker mediating nitrative stress [23]), which was reversed by LY333531 (Fig. 6*F*).

DISCUSSION

In the current study, we have demonstrated that hyperglycemia-induced cardiac PKCβ$_2$ activation requires caveolae. We provide evidence that excessive PKCβ$_2$ activation is associated with reduced Cav-3 expression, contributing

TABLE 1
General characteristics and echocardiographic assessment of left ventricle dimensions and functions in rats

	Control	Diabetes	Diabetes plus LY333531
Blood glucose (mmol/L)	6.26 ± 0.53	28.24 ± 4.64**	27.32 ± 3.43**
Body weight (g)	490.1 ± 14.3	295.4 ± 28.8*	371.1 ± 17.4*
Heart weight (g)	1.66 ± 0.15	1.25 ± 0.18*	1.31 ± 0.16*
Heart weight/body weight (mg/g)	3.39 ± 0.07	4.23 ± 0.06*	3.53 ± 0.08#
HR (bpm)	332 ± 7.8	270 ± 10.8*	286 ± 9.2*
LVIDs (mm)	4.75 ± 0.43	4.68 ± 0.41	4.74 ± 0.49
LVIDd (mm)	8.29 ± 0.53	7.61 ± 0.62	8.13 ± 0.49
FS (%)	42.70 ± 4.13	38.50 ± 5.42	41.53 ± 3.84
IVSs (mm)	2.23 ± 0.16	2.28 ± 0.07	2.27 ± 0.13
IVSd (mm)	1.72 ± 0.05	1.75 ± 0.05	1.73 ± 0.06
LVPWs (mm)	2.90 ± 0.08	2.92 ± 0.07	2.91 ± 0.06
LVPWd (mm)	1.85 ± 0.06	1.91 ± 0.09	1.87 ± 0.08
LVPW (%)	56.76 ± 7.50	52.88 ± 10.03	55.61 ± 4.81
LVVs (μL)	107.6 ± 15.8	109.8 ± 13.7	114.5 ± 11.9
LVVd (μL)	378.7 ± 25.6	315.4 ± 21.8*	380.4 ± 19.7#
EF (%)	71.6 ± 4.7	65.2 ± 5.7	69.9 ± 3.9
IVRT (ms)	21.75 ± 1.25	27.83 ± 1.80*	20.63 ± 1.38#
E velocity (cm/s)	1,340.9 ± 44.6	1,217.8 ± 33.7*	1,331.0 ± 40.8#
A velocity (cm/s)	890.1 ± 37.1	1,023.4 ± 34.7*	917.9 ± 28.9#
E/A ratio	1.49 ± 0.09	1.19 ± 0.05*	1.45 ± 0.085#
SV (μL)	285.7 ± 19.1	230.8 ± 17.9*	279.4 ± 20.8#

Data are means ± SEM. Control or STZ-induced diabetic rats were either untreated or treated with PKCβ inhibitor LY333531 (1 mg/kg/day) by oral gavage for 4 weeks. n = 8. IVSd, diastolic interventricular septal thickness; IVSs, systolic interventricular septal thickness. *$P < 0.05$, **$P < 0.01$ vs. C; #$P < 0.05$ vs. D.

to abnormal Akt/eNOS signaling during hyperglycemia. Inhibition of excessive activation of PKCβ$_2$ by compound LY333531 improves cardiac diastolic function, possibly via attenuation of caveolar dysfunction and rescuing Akt/eNOS/NO function in the diabetic heart. To our best knowledge, this is the first study examining the relationship between PKCβ$_2$ and Cav-3 in cardiomyocytes subjected to hyperglycemic conditions.

It is well established that chronic hyperglycemia induces abnormal activation of PKC, which contributes to diabetic cardiovascular complications (37,38). However, the PKC-signaling pathway is complicated by numerous isoforms, each with varying cellular distribution and opposing function at times (39). The PKCβ$_2$ isoform is most frequently implicated in diabetic cardiovascular complications (5–8). Our current study further confirmed that PKCβ$_2$, but not PKCβ$_1$, is excessively activated in the diabetic heart. Although the precise mechanisms by which hyperglycemia induces PKCβ$_2$ activation in cardiomyocytes are not fully understood, evidence supports the vital role of caveolae (the specialized plasma membrane microdomains modulating signaling transduction pathways of molecules docked within them [16]) in hyperglycemia-induced PKCβ$_2$ activation. This is well supported by our immunoprecipitation and immunofluorescence studies demonstrating that hyperglycemia increased the association and colocalization of PKCβ$_2$ and Cav-3. Caveolar disruption by methyl-β-cyclodextrin (33) suppressed hyperglycemia-induced PKCβ$_2$ activation in isolated cardiomyocytes. Cav-3 knockdown by siRNA prevented augmented PKCβ$_2$ phosphorylation in H9C2 cells exposed to HG, suggesting that Cav-3 is required specifically for hyperglycemia-induced PKCβ$_2$ activation in cardiomyocytes.

Cav-3 is the predominant cardiomyocyte Cav isoform essential for caveolar function. In the current study, we demonstrated that cardiomyocyte Cav-3 expression increased 6–12 h after HG exposure but reduced to basal levels within 24 h and progressively further reduced to lower than basal levels after 36–48 h of HG exposure. The initial increase in Cav-3 expression after HG exposure observed in our study is an acute response to the calorie surplus similar to that reported by other researchers (40). The significant reduction of Cav-3 expression in cardiomyocytes after prolonged HG exposure is consistent with our results from the intact rats, which showed that Cav-3 expression was decreased in isolated cardiomyocytes from rats of 8- and 5-week duration of diabetes. Loss of Cav-3 expression results in cardiomyopathy (41), and reduction in cardiac Cav3 protein expression is highly correlated with reduction in LV FS in mice with constitutive overexpression of A1-adenosine receptor–induced cardiac dilatation and dysfunction and with makers of heart failure phenotype in humans (42). Our study results suggest that excess PKCβ$_2$ activation contributes to attenuated Cav-3 expression in the diabetic heart, as inhibition of PKCβ$_2$ activation by CGP53353 or siRNA-mediated PKCβ$_2$ expression knockdown prevented the decline of Cav-3 expression in cells exposed to HG. LY333531 treatment ameliorated diabetic heart caveolae dysfunction.

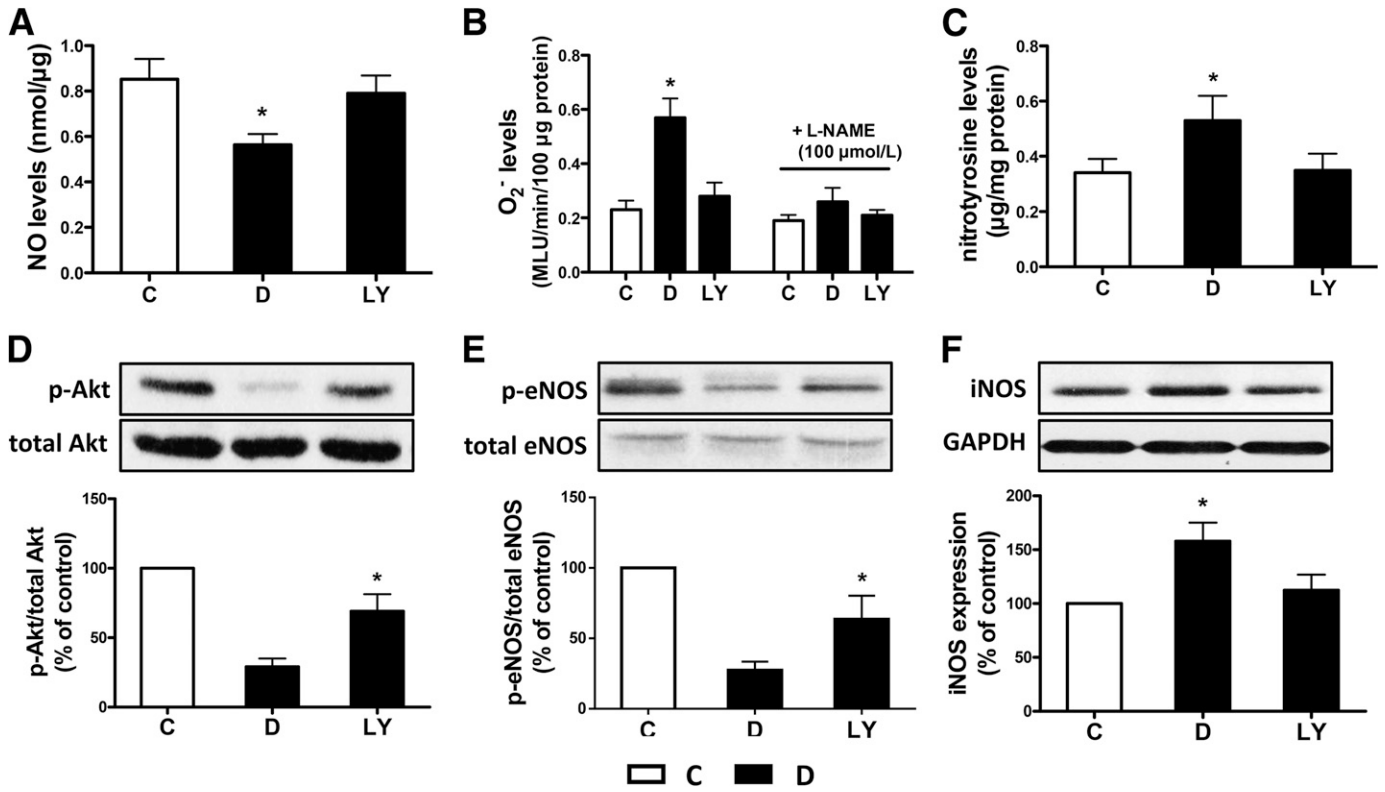

FIG. 6. Effects of PKCβ inhibitor (LY333531) treatment upon the levels of NO, O_2^-, nitrotyrosine, and protein expression of p-Akt, p-eNOS, and iNOS in diabetic myocardium. Controls (C) (□) or rats with STZ-induced diabetes were treated with PKCβ inhibitor LY333531 (1 mg/kg/day) (D+LY) or control (D) (■) by oral gavage for 4 weeks. Effects of LY333531 upon myocardial NO levels (*A*), O_2^- levels in the absence and presence of L-NAME (*B*), and nitrotyrosine levels (*C*). Representative Western blot of p-Akt compared with total Akt (*D*), p-eNOS compared with total eNOS (*E*), and iNOS with glyceraldehyde-3-phosphate dehydrogenase (GAPDH) as loading control (*F*). All results are expressed as means ± SEM. $n = 7$. *$P < 0.05$ vs. all other groups. MLU, mean light unit.

PKCβ$_2$ activation likely exerts adverse effects in the diabetic heart via alteration of the Akt/eNOS signaling pathway, which is modulated by Cavs (34). Although Cav-1 negatively regulates eNOS in cardiovascular tissues (43,44), the colocalization of Cav-3 and eNOS may facilitate eNOS activation by both cell surface receptors and cellular surface NO release for intercellular signaling in cardiomyocytes (17). This is supported by our findings that disruption of caveolae function by methyl-β-cyclodextrin or Cav-3 siRNA prevented Akt phosphorylation and suppressed eNOS phosphorylation in cardiomyocytes. Additionally, hyperglycemia decreased phosphorylated Akt and eNOS both in isolated cardiomyocytes and in diabetic heart tissues, leading to decreased myocardial NO levels, reduced Cav-3 levels, and increased Cav-1 cardiac levels. Inhibition of PKCβ$_2$ activation suppressed or abrogated these alterations. Therefore, inhibition of PKCβ$_2$ activation may rescue proper Akt/eNOS/NO signaling in the diabetic heart via Cav regulation.

Previous studies have demonstrated involvement of increased iNOS expression with cardiovascular abnormalities in STZ-induced diabetic rats (23,45). Our study confirms increased iNOS cardiac content in diabetic rats, an adverse mediator of nitrative stress (23), and increased nitrotyrosine was also demonstrated in diabetic heart tissue. The NOS inhibitor L-NAME blocked diabetes-induced augmentation of O_2^- levels, indicating eNOS uncoupling, which is in line with a recent study in STZ-induced diabetic mice (46). Furthermore, treatment of diabetic rats with LY333531 inhibited cardiac iNOS expression and reduced both nitrotyrosine and O_2^- production. Diabetes is associated with decreased NO levels and increased O_2^- and nitrotyrosine production (14,35), which are implicated with oxidative/nitrative stress and eNOS uncoupling. Our study provides direct evidence showing that inhibition of PKCβ$_2$ activation can mitigate oxidative/nitrative stress and eNOS uncoupling.

Initial LV diastolic dysfunction, reduced contractility, and prolonged diastole are the hallmarks of diabetic cardiomyopathy (47,48). In the current study, diabetes significantly reduced E/A ratio, which was concomitant with significantly increased IVRT and decreased LVVd and SV but did not alter FS, FLVPW, or EF. Such data indicate that myocardial diastolic (but not systolic) dysfunction occurs in 5-week STZ-induced diabetes rats, which can be ameliorated by LY333531. Our findings are in general agreement with the findings of Mihm et al. (26), who conducted a series study in similar STZ diabetic rats and showed that diastolic dysfunction occurred early during the course of the disease, which progressed to LV dilation reflected as increases in LVIDd and LVIDs with concomitant increase in LV luminal area and systolic dysfunction reflected as reduction in LV FS 35 days after STZ injection and onward. It should be noted that the E/A ratio derived from the conventional Doppler echocardiography as used in our current study is not a load-independent parameter and may have inherent limitations, e.g., the peak E wave velocity can be highly dependent upon HR (26), while the HR in the diabetic rats was lower than that in the control group (Table 1). The newly developed Doppler tissue echocardiography (DTE) can acquire myocardial wall and mitral annular velocity online, and the early diastolic annular velocity measured using DTE has been reported to be a preload independent index for evaluating LV diastolic function. A combination of

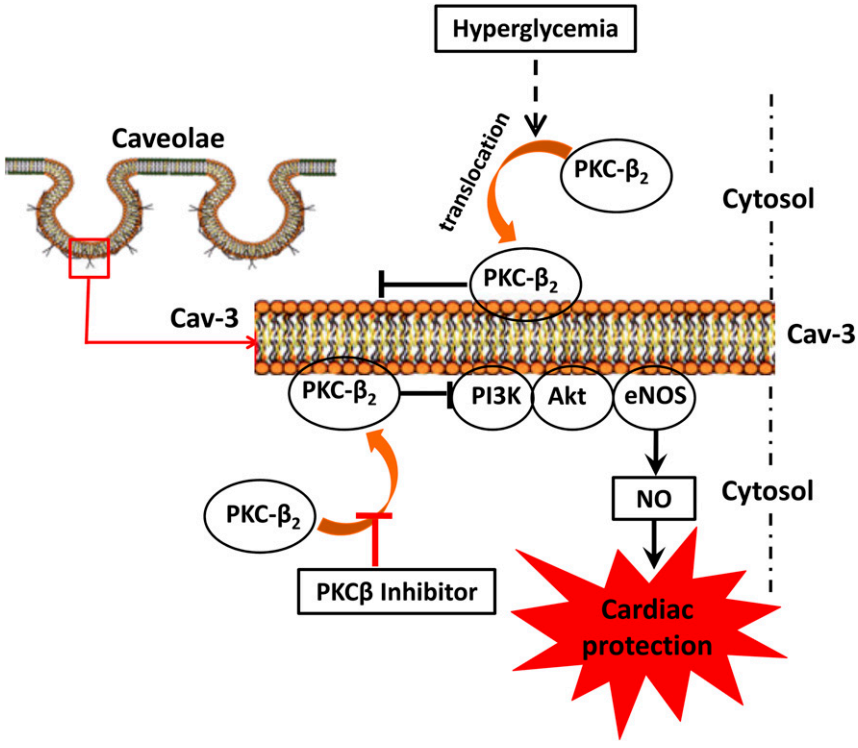

FIG. 7. Schematic depicting hyperglycemia-induced PKCβ2 activation effects upon Cav-3–modulated Akt/eNOS signaling pathway. Cardiomyocyte caveolae are required for hyperglycemia-induced PKCβ$_2$ activation (translocation from cytosol to caveolae membrane). Excessive PKCβ$_2$ activation decreased Cav-3 expression, impairing the Akt/eNOS signaling pathway. Solid arrows depict stimulation, while transverse "T" shape indicates inhibition. PI3K, phosphatidylinositol 3-kinase.

DTE-derived E′/A′ ratio and the mitral inflow patterns (E/A ratio) obtained by conventional Doppler echocardiography in future studies should help to provide better estimations of diastolic dysfunction. However, the significant reduction of E/A ratio as a consequence of significant reduction of E velocity and significant enhancement of A velocity in combination with concomitant increase in IVRT and reductions in LVVD and SV in the diabetic group could jointly suggest diastolic dysfunction in the current study. LY333531 treatment in diabetic rats did not affect HR but corrected all of the above changes, suggesting that LY333531 treatment prevented the development of diastolic dysfunction. Future functional study with cardiomyocytes isolated from rodents in various stages of diabetes will help establish the relative contribution of the slowing in cardiomyocyte relaxation time and LV stiffness (due to fibrosis) to the development of diastolic dysfunction.

In summary, our study demonstrates that hyperglycemia-induced PKCβ_2 activation is associated with caveolar dysfunction and, consequently, deranged Akt/eNOS signaling (Fig. 7). Inhibition of PKCβ_2 activation attenuated cardiac diastolic dysfunction by restoring Cav-3 expression and subsequently rescuing Akt/eNOS/NO signaling. PKCβ_2 blockade may therefore represent a novel therapeutic avenue in the treatment of diabetic cardiomyopathy.

ACKNOWLEDGMENTS

This study was supported by a grant from the National Natural Science Foundation of China (NSFC 81270899) and by General Research Fund grants (784011M and 782910M) from the Research Grants Council of Hong Kong.

No potential conflicts of interest relevant to this article were reported.

S.L. performed the study and wrote the manuscript. H.L., J.X., Y.L., and X.G. performed the study. J.W., K.F.J.N., W.B.L., X.-l.M., and B.R. contributed to data analysis and interpretation. M.G.I. reviewed and approved the research protocol. Z.X. reviewed and approved the research protocol and wrote the manuscript. Z.X. is the guarantor of this work and, as such, had full access to all the data in the study and takes responsibility for the integrity of the data and the accuracy of the data analysis.

REFERENCES

1. Khavandi K, Khavandi A, Asghar O, et al. Diabetic cardiomyopathy—a distinct disease? Best Pract Res Clin Endocrinol Metab 2009;23:347–360
2. Zarich SW, Nesto RW. Diabetic cardiomyopathy. Am Heart J 1989;118:1000–1012
3. Kim DH, Kim YJ, Chang SA, et al. The protective effect of thalidomide on left ventricular function in a rat model of diabetic cardiomyopathy. Eur J Heart Fail 2010;12:1051–1060
4. Ni Q, Wang J, Li EQ, et al. Study on the protective effect of shengmai san (see text) on the myocardium in the type 2 diabetic cardiomyopathy model rat. J Tradit Chin Med 2011;31:209–219
5. Xia Z, Kuo KH, Nagareddy PR, et al. N-acetylcysteine attenuates PKCbeta2 overexpression and myocardial hypertrophy in streptozotocin-induced diabetic rats. Cardiovasc Res 2007;73:770–782
6. Liu Y, Lei S, Gao X, et al. PKCβ inhibition with ruboxistaurin reduces oxidative stress and attenuates left ventricular hypertrophy and dysfunction in rats with streptozotocin-induced diabetes. Clin Sci (Lond) 2012;122:161–173
7. Gurusamy N, Watanabe K, Ma M, et al. Inactivation of 14-3-3 protein exacerbates cardiac hypertrophy and fibrosis through enhanced expression of protein kinase C beta 2 in experimental diabetes. Biol Pharm Bull 2005;28:957–962
8. Way KJ, Isshiki K, Suzuma K, et al. Expression of connective tissue growth factor is increased in injured myocardium associated with protein kinase C beta2 activation and diabetes. Diabetes 2002;51:2709–2718
9. Wei L, Yin Z, Yuan Y, et al. A PKC-beta inhibitor treatment reverses cardiac microvascular barrier dysfunction in diabetic rats. Microvasc Res 2010;80:158–165
10. Connelly KA, Kelly DJ, Zhang Y, et al. Inhibition of protein kinase C-beta by ruboxistaurin preserves cardiac function and reduces extracellular matrix production in diabetic cardiomyopathy. Circ Heart Fail 2009;2:129–137
11. Clarke M, Dodson PM. PKC inhibition and diabetic microvascular complications. Best Pract Res Clin Endocrinol Metab 2007;21:573–586
12. Simpson PC. Beta-protein kinase C and hypertrophic signaling in human heart failure. Circulation 1999;99:334–337
13. Naruse K, Rask-Madsen C, Takahara N, et al. Activation of vascular protein kinase C-beta inhibits Akt-dependent endothelial nitric oxide synthase function in obesity-associated insulin resistance. Diabetes 2006;55:691–698
14. Ren J, Duan J, Thomas DP, et al. IGF-I alleviates diabetes-induced RhoA activation, eNOS uncoupling, and myocardial dysfunction. Am J Physiol Regul Integr Comp Physiol 2008;294:R793–R802
15. Rybin VO, Xu X, Steinberg SF. Activated protein kinase C isoforms target to cardiomyocyte caveolae : stimulation of local protein phosphorylation. Circ Res 1999;84:980–988
16. Panneerselvam M, Patel HH, Roth DM. Caveolins and heart diseases. Adv Exp Med Biol 2012;729:145–156
17. Feron O, Balligand JL. Caveolins and the regulation of endothelial nitric oxide synthase in the heart. Cardiovasc Res 2006;69:788–797
18. Kempf T, Wollert KC. Nitric oxide and the enigma of cardiac hypertrophy. Bioessays 2004;26:608–615
19. Fujita T, Otsu K, Oshikawa J, et al. Caveolin-3 inhibits growth signal in cardiac myoblasts in a Ca2+-dependent manner. J Cell Mol Med 2006;10:216–224
20. Penumathsa SV, Thirunavukkarasu M, Zhan L, et al. Resveratrol enhances GLUT-4 translocation to the caveolar lipid raft fractions through AMPK/Akt/eNOS signalling pathway in diabetic myocardium. J Cell Mol Med 2008;12:2350–2361
21. Penumathsa SV, Thirunavukkarasu M, Samuel SM, et al. Niacin bound chromium treatment induces myocardial Glut-4 translocation and caveolar interaction via Akt, AMPK and eNOS phosphorylation in streptozotocin induced diabetic rats after ischemia-reperfusion injury. Biochim Biophys Acta 2009;1792:39–48
22. Gálvez MI. Protein kinase C inhibitors in the treatment of diabetic retinopathy. Review. Curr Pharm Biotechnol 2011;12:386–391 [Review]
23. Nagareddy PR, Soliman H, Lin G, et al. Selective inhibition of protein kinase C beta(2) attenuates inducible nitric oxide synthase-mediated cardiovascular abnormalities in streptozotocin-induced diabetic rats. Diabetes 2009;58:2355–2364
24. Ishii H, Jirousek MR, Koya D, et al. Amelioration of vascular dysfunctions in diabetic rats by an oral PKC beta inhibitor. Science 1996;272:728–731
25. Gao X, Xu Y, Xu B, et al. Allopurinol attenuates left ventricular dysfunction in rats with early stages of streptozotocin-induced diabetes. Diabetes Metab Res Rev 2012;28:409–417
26. Mihm MJ, Seifert JL, Coyle CM, Bauer JA. Diabetes related cardiomyopathy time dependent echocardiographic evaluation in an experimental rat model. Life Sci 2001;69:527–542
27. Wang T, Qiao S, Lei S, et al. N-acetylcysteine and allopurinol synergistically enhance cardiac adiponectin content and reduce myocardial reperfusion injury in diabetic rats. PLoS ONE 2011;6:e23967
28. Luo T, Xia Z, Ansley DM, et al. Propofol dose-dependently reduces tumor necrosis factor-alpha-Induced human umbilical vein endothelial cell apoptosis: effects on Bcl-2 and Bax expression and nitric oxide generation. Anesth Analg 2005;100:1653–1659
29. Li YL, Gao L, Zucker IH, Schultz HD. NADPH oxidase-derived superoxide anion mediates angiotensin II-enhanced carotid body chemoreceptor sensitivity in heart failure rabbits. Cardiovasc Res 2007;75:546–554
30. Li JM, Shah AM. Mechanism of endothelial cell NADPH oxidase activation by angiotensin II. Role of the p47phox subunit. J Biol Chem 2003;278:12094–12100
31. Lei S, Liu Y, Liu H, Yu H, Wang H, Xia Z. Effects of N-acetylcysteine on nicotinamide dinucleotide phosphate oxidase activation and antioxidant status in heart, lung, liver and kidney in streptozotocin-induced diabetic rats. Yonsei Med J 2012;53:294–303
32. Zhang Y, Peng F, Gao B, Ingram AJ, Krepinsky JC. High glucose-induced RhoA activation requires caveolae and PKCβ1-mediated ROS generation. Am J Physiol Renal Physiol 2012;302:F159–F172
33. Christian AE, Haynes MP, Phillips MC, Rothblat GH. Use of cyclodextrins for manipulating cellular cholesterol content. J Lipid Res 1997;38:2264–2272
34. Krajewska WM, Masłowska I. Caveolins: structure and function in signal transduction. Cell Mol Biol Lett 2004;9:195–220
35. Jin HR, Kim WJ, Song JS, et al. Intracavernous delivery of a designed angiopoietin-1 variant rescues erectile function by enhancing endothelial

regeneration in the streptozotocin-induced diabetic mouse. Diabetes 2011;60:969–980
36. Cheng YS, Dai DZ, Ji H, Zhang Q, Dai Y. Sildenafil and FDP-Sr attenuate diabetic cardiomyopathy by suppressing abnormal expression of myocardial CASQ2, FKBP12.6, and SERCA2a in rats. Acta Pharmacol Sin 2011;32:441–448
37. Geraldes P, King GL. Activation of protein kinase C isoforms and its impact on diabetic complications. Circ Res 2010;106:1319–1331
38. Danis RP, Sheetz MJ. Ruboxistaurin: PKC-beta inhibition for complications of diabetes. Expert Opin Pharmacother 2009;10:2913–2925
39. Mellor H, Parker PJ. The extended protein kinase C superfamily. Biochem J 1998;332:281–292
40. Gómez-Ruiz A, de Miguel C, Campión J, Martínez JA, Milagro FI. Time-dependent regulation of muscle caveolin activation and insulin signalling in response to high-fat diet. FEBS Lett 2009;583:3259–3264
41. Woodman SE, Park DS, Cohen AW, et al. Caveolin-3 knock-out mice develop a progressive cardiomyopathy and show hyperactivation of the p42/44 MAPK cascade. J Biol Chem 2002;277:38988–38997
42. Feiner EC, Chung P, Jasmin JF, et al. Left ventricular dysfunction in murine models of heart failure and in failing human heart is associated with a selective decrease in the expression of caveolin-3. J Card Fail 2011;17:253–263
43. Elçioğlu KH, Kabasakal L, Cetinel S, Conturk G, Sezen SF, Ayanoğlu-Dülger G. Changes in caveolin-1 expression and vasoreactivity in the aorta and corpus cavernosum of fructose and streptozotocin-induced diabetic rats. Eur J Pharmacol 2010;642:113–120
44. Lam TY, Seto SW, Lau YM, et al. Impairment of the vascular relaxation and differential expression of caveolin-1 of the aorta of diabetic +db/+db mice. Eur J Pharmacol 2006;546:134–141
45. Nagareddy PR, Xia Z, McNeill JH, MacLeod KM. Increased expression of iNOS is associated with endothelial dysfunction and impaired pressor responsiveness in streptozotocin-induced diabetes. Am J Physiol Heart Circ Physiol 2005;289:H2144–H2152
46. Roe ND, Thomas DP, Ren J. Inhibition of NADPH oxidase alleviates experimental diabetes-induced myocardial contractile dysfunction. Diabetes Obes Metab 2011;13:465–473
47. Norby FL, Aberle NS 2nd, Kajstura J, Anversa P, Ren J. Transgenic overexpression of insulin-like growth factor I prevents streptozotocin-induced cardiac contractile dysfunction and beta-adrenergic response in ventricular myocytes. J Endocrinol 2004;180:175–182
48. Palmieri V, Capaldo B, Russo C, et al. Uncomplicated type 1 diabetes and preclinical left ventricular myocardial dysfunction: insights from echocardiography and exercise cardiac performance evaluation. Diabetes Res Clin Pract 2008;79:262–268